Journal of Structural Geology 37 (2012) 53–64

Contents lists available at SciVerse ScienceDirect

Journal of Structural Geology

journal homepage: www.elsevier.com/locate/jsg

Growth processes, dimensional parameters and scaling relationships of two conjugate sets of compactive shear bands in porous carbonate grainstones, Favignana Island, Italy

E. Tondi [a,*], A. Cilona [a], F. Agosta [b], A. Aydin [c], A. Rustichelli [a], P. Renda [d], G. Giunta [d]

[a] Geology Division, School of Science and Technology, University of Camerino, 62032, Camerino, MC, Italy
[b] Department of Geological Sciences, University of Basilicata, Potenza, Italy
[c] Department of Geological and Environmental Sciences, Stanford University, Stanford, USA
[d] Dipartimento di Scienze della Terra e del Mare, Università di Palermo, Palermo, Italy

ARTICLE INFO

Article history:
Received 2 November 2011
Received in revised form
30 January 2012
Accepted 2 February 2012
Available online 15 February 2012

Keywords:
Offshore Sicily
Pleistocene deposits
Compaction bands
Deformation bands
Fault scaling

ABSTRACT

Three main sets of deformation bands are identified in the Lower Pleistocene carbonate grainstones of Favignana Island (Italy). A bedding-parallel set is interpreted to contain compaction bands, based on the lack of evidence for shear. The other two sets are oriented at a high-angle to bedding, forming a conjugate pair comprised of compactive strike-slip shear bands. In this study, we focus on the compactive shear bands documenting their development, as well as analyzing their dimensional parameters and scaling relationships.

Single compactive shear bands are thin, tabular zones with porosity less than the surrounding host rocks, and have thicknesses and displacements on the order of a few mm. The growth process for these structures involves localizing further deformation within zones of closely-spaced compactive shear bands and, possibly, along continuous slip surfaces within fault rocks overprinting older zones of bands. During growth, single bands, zones of bands and faults can interact and link, producing larger structures. The transitions from one growth step to another, which are controlled by changes in the deformation behavior (i.e. banding vs. faulting), are recorded by different values of the dimensional parameters for the structures (i.e. length, thickness and displacement). These transitions are also reflected by the ratios and distributions of the dimensional parameters. Considering the lesser porosity values of the structures with respect to the host rock, the results of this contribution could be helpful for mapping, assessing, and simulating carbonate grainstone reservoirs with similar structures.

1. Introduction

Deformation bands are tabular zones mm- to-cm thick, which accommodate shear and/or volumetric strain in porous rocks and sediments (Engelder, 1974; Aydin, 1978; Aydin and Johnson, 1978; Antonellini and Aydin, 1994; Aydin et al., 2006; Eichhubl et al., 2010; Fossen et al., 2011). Many natural examples of deformation bands are reported from siliciclastic sediments (Fossen et al., 2007; and references therein). In contrast, only a few field examples of deformation bands are described in porous limestones (Micarelli et al., 2006; Tondi et al., 2006a; Tondi, 2007; Rath et al., 2011). Deformation bands are easily recognizable because of their lighter-colour and positive relief with respect to the parent rocks. These field characteristics are strictly related to the deformation mechanisms that modify the grain sizes and porosity values within the bands. Microscopic observations of natural deformation bands, as well as those obtained from experiments on high-porosity limestones (Vajdova et al., 2004; Baxevanis et al., 2006; Baud et al., 2009; Vajdova et al., 2010; Zhu et al., 2010; Cilona et al., Submitted for publication; Vajdova et al., submitted for publication), show a variety of mechanisms responsible for their nucleation and development: (i) grain sliding with rotation and pore collapse; (ii) grain fracturing; and (iii) pressure solution. The first two mechanisms are responsible for the formation of narrow tabular deformation bands with volumetric and shear strain. If the volumetric component of this deformation is negative, the product is known as a compactive (or compactional) shear band (Aydin et al., 2006; Tondi et al., 2006a; Fossen et al., 2007; Tondi, 2007), granulation seams (Pittman, 1981) or disaggregation bands (Fossen et al., 2007). At more advanced stages of deformation, within the

* Corresponding author.
E-mail address: emanuele.tondi@unicam.it (E. Tondi).

0191-8141/$ – see front matter © 2012 Elsevier Ltd. All rights reserved.
doi:10.1016/j.jsg.2012.02.003

already compacted bands, pressure solution is the main process responsible for grain-size reduction (Tondi, 2007), which could be also defined dissolution/cementation bands sensu Fossen et al. (2007). Eventually, further deformation facilitates slip along pre-existing stylolites and enhances the accumulation of a larger displacement along discrete shear planes (Aydin et al., 2006; Tondi et al., 2006a). Mechanical twinning of calcite crystals (Ferrill and Groshong, 1993) and precipitation of dissolved solids in the nearby pores are processes also documented within deformation bands in porous limestones (Tondi et al., 2006a; Tondi, 2007; Baud et al., 2009; Vajdova et al., 2010; Rath et al., 2011).

The transition from one deformation behavior to another (i.e. banding vs. faulting) is likely controlled by changes of the material properties within the bands; the resulting mechanical instability is often accompanied by progressive evolution of the tectonic structures (Aydin and Johnson, 1983; Shipton et al., 2005). In porous rocks, deformation first occurs in the form of single compactive shear bands, evolves continuously forming zones of multiple compactive shear bands and, eventually, faults composed of discrete, sharp, more or less planar discontinuities and fault rocks (i.e. breccia and gouge).

The aim of this study is to investigate both dimensional parameters and scaling relationships of single compactive shear bands, zones of compactive shear bands and strike-slip faults in porous carbonate grainstones. Many excellent outcrops of Favignana Island (Egadi Islands, western Sicily) expose a 21–23 m-thick Lower-Pleistocene porous carbonate grainstones crosscut by the aforementioned tectonic structures. There, we collected detailed data related to length, thickness and amount of slip along structures as well as to investigate their detailed geometries, kinematics and growth processes. Previous works on fault scaling relationships provide a window into the mechanics of brittle strain localization in compact and porous rocks (Cowie and Scholz, 1992; Dawers et al., 1993; Willemse et al., 1996; Scholz, 2002; de Joussineau and Aydin, 2007; Fossen et al., 2007; Schultz et al., 2008). In particular, the previous data from porous rocks pertain primarily to displacement–length (D–L) and displacement-damage zone thickness (D–T) scaling relations of deformation bands in sandstones (Fossen and Hesthammer, 1997; Shipton and Cowie, 2001; Wibberley et al., 2000; Shipton et al., 2005; and Fossen et al., 2007 and the references therein). Data presented in this paper provide a new insight into the evolution of statistical parameters of shear bands, which may be useful for an improved understanding of faults in porous carbonate rocks and characterization of carbonate reservoirs (cf. Agosta et al., 2010).

2. Geological framework

Favignana is the largest of the Egadi Islands, and is located in NW Sicily along the southern edge of the Tyrrhenian Sea (Fig. 1a). This area represents the westernmost, and most external, sector of the Sicilian orogenic belt, which is mainly comprised of south-verging, Neogene fold-thrust tectonic elements (Fig. 1a; Scandone et al., 1974; Giunta et al., 2000).

The most recent faults of NW Sicily (Nigro et al., 2000; Renda et al., 2000; Gueguen et al., 2002; Giunta et al., 2009) form a grid of high-angle strike-slip structures roughly oriented either W-NW (right-lateral) or N-NE (left-lateral). The kinematics of these two sets of strike-slip faults is compatible to the current regional stress field, which is characterized by a NW-SE oriented, greatest horizontal compression direction (Giunta et al., 2004; Tondi et al., 2006b).

At Favignana Island (Fig. 1b), deformed Triassic to Miocene platform carbonates, which pass upwards into deep-water marls and limestones, are the basement units underlying Plio-Pleistocene marine deposits (Abate et al., 1995, 1997; Incandela, 1995; Tavarnelli et al., 2003). These marine deposits are comprised of Upper Pliocene shales overlain by 20–25 m thick, Lower Pleistocene carbonate grainstones (Fig. 1b).

2.1. Lower Pleistocene carbonate grainstones

The yellowish carbonate grainstones of Favignana are Lower Pleistocenic in age. The grainstones are characterized by beds dipping: 5°–10° ESE, and a bed thickness ranging between 20 cm and 100 cm. The mean thickness of the whole Lower Pleistocene succession is nearly 21 m at Cala San Nicola and 23 m at Cala Rossa (Fig. 1b and Fig. 2). The maximum burial depth experienced by the carbonate grainstones is estimated to be between 0 and 30 m (Abate et al., 1995, 1997).

Based upon their grain size, sorting, sedimentary/biogenic structures and amount of matrix and cement, as well as the widespread erosional flooding surfaces, we distinguish up to seven different lithofacies (Fig. 2). In general, the carbonate grainstones are mainly comprised of bioclasts (i.e. *Vermetus*, *Serpula*, lamellibanches, echinoids, algae and corals) ranging in size from sub-millimeter to centimeter (Fig. 2b). The amount of matrix and calcite cement vary significantly among the different lithofacies.

Thin-section observations are consistent with presence of intergranular and intragranular porosity within the carbonate grainstones. Generally, well-developed intergranular pores form

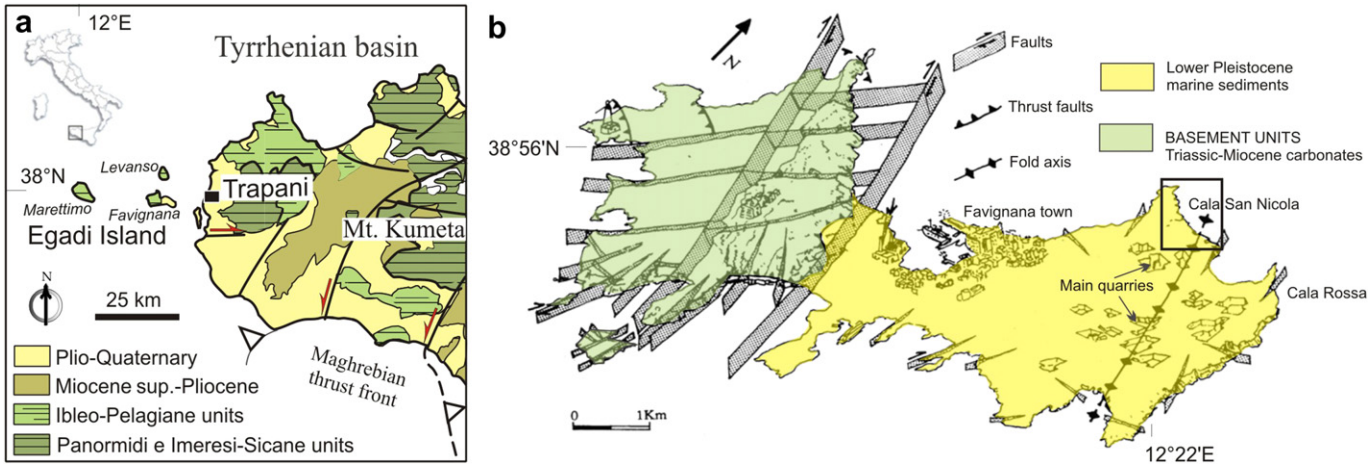

Fig. 1. (a) Geological setting of western Sicily and (b) of Favignana Island. The location of the study area is marked with a black rectangle.

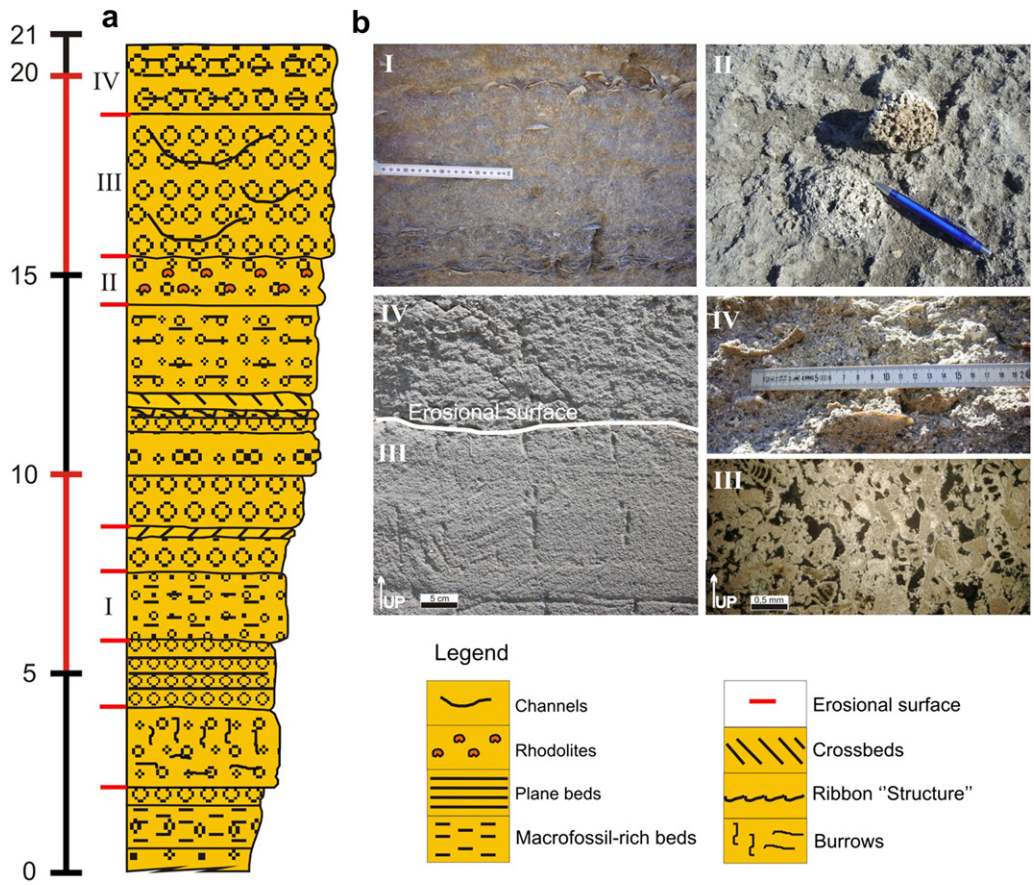

Fig. 2. (a) Stratigraphic section of the carbonate grainstones cropping out at Cala San Nicola with scale in meters and circle sizes proportional to grain sizes. (b) Four field photos of the main lithofacies and one photomicrograph referenced by Roman numerals to lithofacies in the stratigraphic section.

a connected network in 2D. Both shape and size of these pores change according to the grain size and sorting in the rock (Fig. 2b). Intergranular pores can reach a few mm in diameter in the very coarse-grained lithofacies. The overall host rock porosity measured by both image analysis (2D) and laboratory measurements of representative cylindrical cores (3D, Patrick Baud's personal communication) ranges between 30% (lithofacies III, Fig. 2) and 50% (lithofacies IV, Fig. 2). Microsparry cement is always present, in small amounts, at the grain contacts and/or within intragranular porosity. In addition, syntaxial overgrowth cement is present around echinoid plates and spines.

3. Field data

The compactive shear bands and strike-slip faults in Favignana, the subject of this study, are similar to those reported by Tondi (2007) within the marine deposits, of Lower Pleistocene age, cropping out in the coastal plain of Castelluzzo (San Vito Lo Capo Peninsula, NW Sicily). At both localities, the compactive shear bands occur in coeval marine deposits overlying the Mesozoic-Cenozoic basement, and show similar geometries and kinematics. For this reason, we rely on the observation and discussion provided by Tondi (2007) about the microstructural and textural characteristics of the bands, as well as on the micromechanical processes involving pore collapse and pressure solution responsible for their formation. At Favignana, thanks to the magnificent and widespread exposures, the field work focused on: (i) geometry, (ii) kinematics, (iii) dimensional parameters (i.e. length, thickness and amount of displacement) of the two sets of compactive shear bands, zones of compactive shear bands and well-developed faults with slip surfaces and fault rocks. In the following text, the latter elements, for the sake of simplicity, will be referred to as faults. Field data were then used to compute the scaling relationships among the different parameters for single bands, zones of bands and faults. The field work was conducted at Cala San Nicola (Fig. 1b), where the thickest and most homogenous Pleistocene carbonate lithofacies crop out extensively (III, Fig. 2). There, several scan lines and detailed structural maps at a 1:1 scale were constructed during several field campaigns.

3.1. Geometry and kinematics

At Cala San Nicola (Fig. 1b), we identified three different sets of deformation bands. One of these sets occurs parallel to bedding (Fig. 3), and is mainly in the coarser grained and more porous carbonate beds (lithofacies IV, Fig. 2). The bed-parallel bands do not show any amount of visible shearing, and are reminiscent of the compaction bands documented in the Majella Mountain area, central Italy (Tondi et al., 2006a; Antonellini et al., 2008; Agosta et al., 2009). Given the lack of evidence for deformation related to shear, these structures were not examined as part of the present study. The two sets of high-angle to bedding deformation bands consist of compactive shear bands, which are either single bands or zones of bands (Fig. 4a and b). Faults including compactive shear bands with continuous slip surfaces, and the associated cataclastic fault rock, mark an advanced stage of deformation within this carbonate grainstone (Fig. 4c).

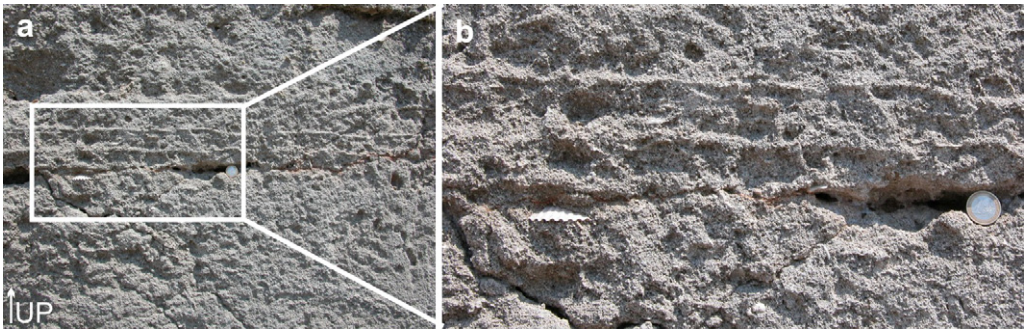

Fig. 3. (a) Field photographs of bed-parallel deformation bands developed with the lithofacies IV of the carbonate grainstones, (b) enlarged area shown by rectangle in (a).

The two sets of compactive shear bands have indicators showing strike-slip motion and mutually crosscutting relationships, indicating coeval development (Fig. 5). These two sets form one pair of conjugate strike-slip faults oriented N-S and NW-SE, respectively. The NW-striking features are characterized by a right-lateral sense of slip, whereas the N-S striking ones by left-lateral motions. In the study area, the two sets of compactive shear bands crop out as (i) isolated, (ii) interacting and, (iii) linking structures. As shown in Fig. 6a, the interaction and linkage among different bands occurs in different manners. Secondary features include extensional or contractional jogs (1 and 2 respectively in Fig. 6), eye structures (3 in Fig. 6), as already described in sandstones (Antonellini and Aydin, 1995), and Riedel-like patterns (2 in Fig. 6; cf. Ahlgren, 2001; Katz et al., 2004). All of these types of interaction and coalescence can be observed along single bands (Fig. 6), as well as along zones of bands and faults (Fig. 7). These observations are consistent with both interaction and linkage occurring at almost every stage of deformation, from single banding, through zones of banding, to faulting.

3.2. Dimensional parameters and scaling relationships

Here we focus on the scaling relationships of the dimensional parameters (i.e. length, thickness and displacement) of the two sets of compactive shear bands. We consider these relationships for each structural morphology for each set: single bands, zone of bands, and faults (Table 1).

Even if kinematic markers are not available for all single bands and zones of bands, striations present along the slip surfaces of faults are almost horizontal, indicating predominantly strike-slip kinematics. Consequently, it is assumed that the slip along the faults is equal to the maximum apparent horizontal slip, determined from the displaced markers such as bedding and/or older bands. The apparent displacement of these markers was also used to compute the amount of horizontal displacement across single bands and zones of bands. Where possible, slip was measured at multiple points along individual single bands and zones of bands, and the greatest slip value is considered to correspond to the maximum displacement for a band or zone of bands.

Displacement-distance graphs were constructed across four structures (Fig. 8). The four examples show that maximum displacement values are located, more or less, at midpoint or in the central portion of their profile. The faults in Fig. 8d are an exception because they have a lesser amount of slip with respect to the predicted slip distribution. This lesser slip is related to an observed zone of linkage, similar to the cases documented by Cartwright et al. (1995) and Willemse et al. (1996). The displacement varies along the zones of bands according to the number of single bands that are present (Fig. 9). Along the faults, by contrast, when displacement reaches 20–30 cm, a continuous discrete slip surface is recognizable. Moreover, along the same structures the number of bands does not increase for larger amount of displacement (Fig. 8c). However, we note that a greater number of bands occur in the damage zones of shear band faults with larger slip (Shipton and Cowie, 2003).

The scaling relationships among the three dimensional parameters, length, thickness and displacement, are shown in Fig. 10. The scatter distributions can be fitted by power-law relationships with the R^2 comprised between 0.3 and 0.8. With regards to zones of bands vs. faults, the switch from one power law distribution to another occurs at about 10 cm of thickness, 10 cm of displacement and 8 m of length. However, it should be noted that the lengths distribution contains a lack of data between 5 and 8 m. The aforementioned values can therefore be treated as the threshold values for the transition from banding to slip surfaces and cataclasis and, consequently, the fault development. In Fig. 10c, it is possible to observe two groups of data: (a) single bands and zones of bands show a power-law scaling relation with a slope of $D = 0.5$, and therefore, a dependence of maximum displacement on the square root of the bands length ($D_{max} = aL^{0.5}$); and (b) faults show a power-law scaling relation with a slope of $D = 0.7$.

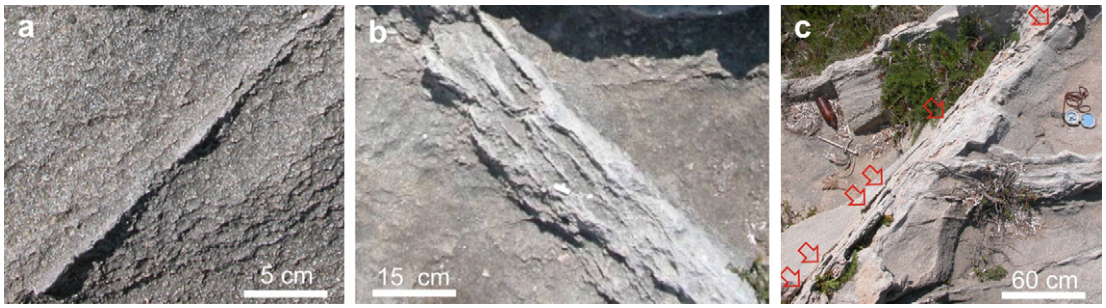

Fig. 4. Field examples of (a) single band; (b) zones of bands; and (c) faults with slip surfaces and fault rocks. In outcrop, slip surfaces are easily recognizable by sharp striated discontinuities, commonly showing a negative relief (marked by red arrows) due to erosion along generally poorly cemented fault rocks (i.e. breccia and/or gouge).

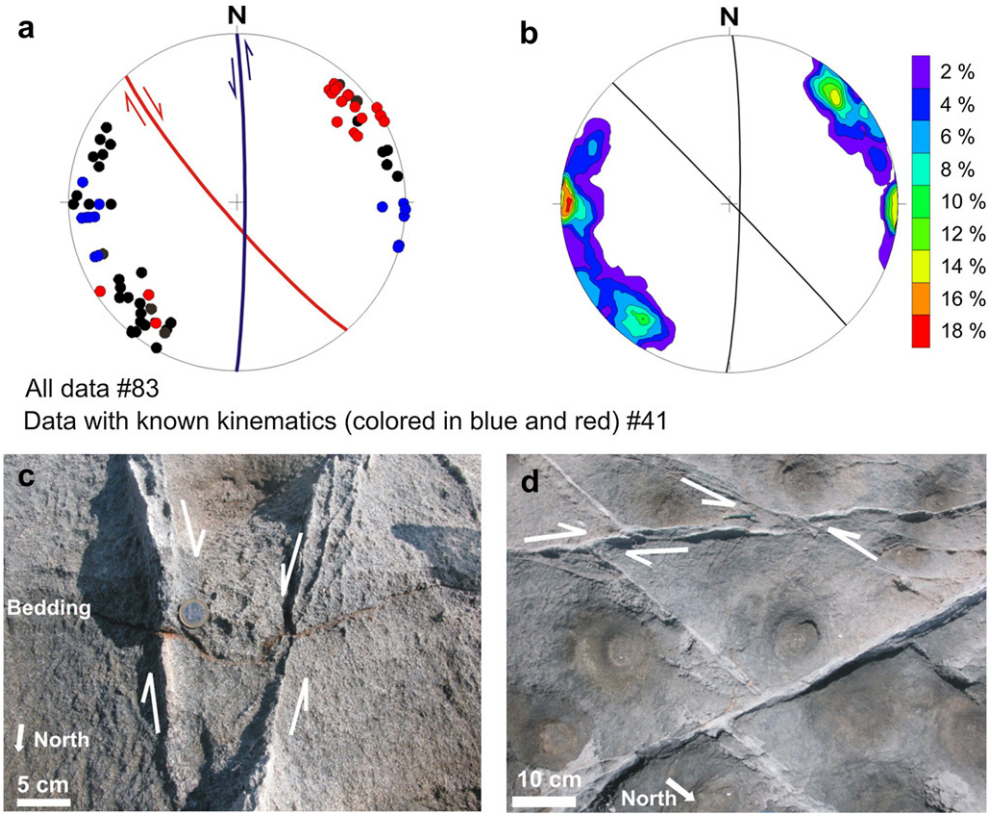

Fig. 5. (a) Plots of the poles and (b) contoured stereonet plots (Schmidt distribution method), lower hemisphere projection, of orientations for compactive shear bands with left (blue)-and right (red)-lateral sense of slip (data with unknown kinematics are in black). The mean great circles are also illustrated. The photos show (c) the displaced sedimentary markers, as well as (d) the mutually crosscutting relationships of the two conjugate sets of compactive shear bands.

In Fig. 11, the cumulative frequency distributions of the three aforementioned dimensional parameters are best fitted by negative power-law (Mandelbrot, 1983):

$$N_{(\geq S)} = aS^{-D} \quad (1)$$

where N is the number of features having a size greater than or equal to S (e.g. the fault length), a is a measurement of the sample size, and the power-law exponent D represents the slope of the best fit line, which some authors interpreted also as the fractal dimension (Childs et al., 1990; Scholz and Cowie, 1990). The analysis shows that for single bands, zones of bands and faults, the presence of data breaks in the thickness and displacement distribution between: (i) single bands and zones of bands, and (ii) faults (Fig. 11a and b).

4. Discussion

At Cala San Nicola, the two sets of compactive shear bands at high-angle to bedding are similar to those documented by Tondi (2007) in carbonate grainstones cropping out at San Vito Lo Capo Peninsula (NW Sicily). These two sets include both single bands and zones of bands. Strike-slip faults are present, as well, and consist of zones of compactive shear bands, discrete slip surfaces and cataclastic fault rocks, and hence represent a more evolved deformation state in the carbonate grainstones. The steep compactive shear bands are coeval and form a pair of conjugate sets striking N-S (left lateral) and NW-SE (right-lateral), respectively. The acute angle defined by the two conjugate sets is about 45° and is likely controlled by the specific deformation mechanism responsible for

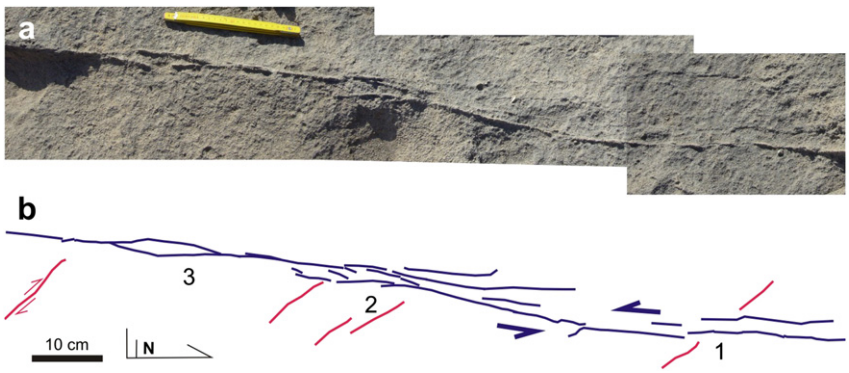

Fig. 6. Different types of interaction and linkage of single compactive shear bands, photograph (a) and map (b). Numbers refer to sites discussed in the text.

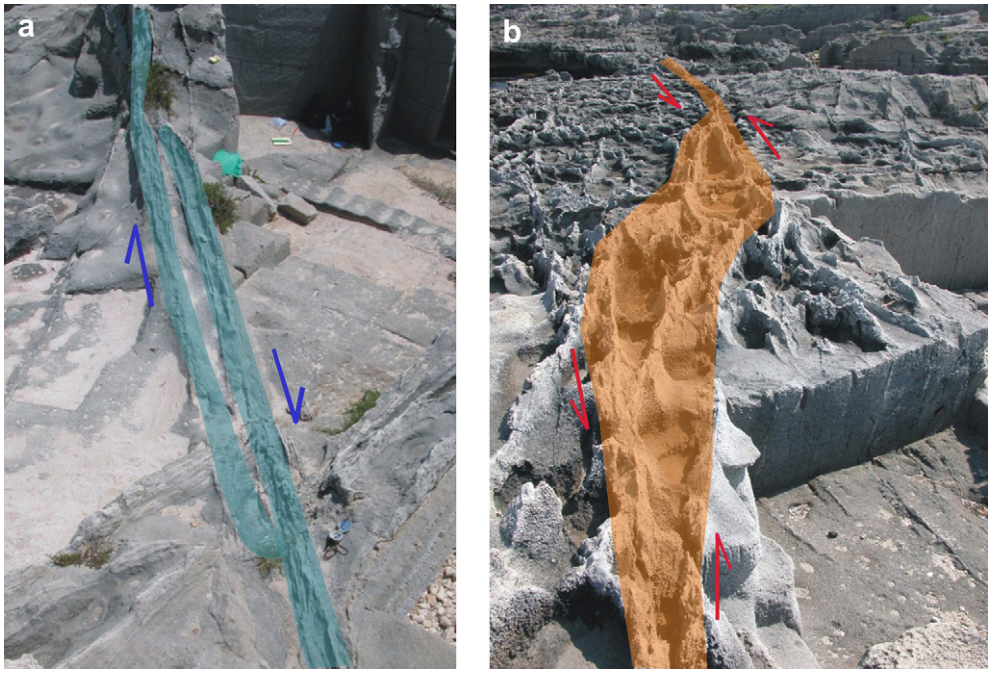

Fig. 7. (a) Extensional jog and (b) contractional jog along a zone of bands and a well-developed strike-slip fault, respectively.

compactive shear banding at an extremely low overburden pressure (Baud et al., 2004; Cilona et al., Submitted for publication).

Compactive shear banding occurs only in rocks and sediments characterized by porosity values greater than about 14% (Aydin and Johnson, 1978; Antonellini and Aydin, 1994; Aydin et al., 2006; Micarelli et al., 2006; Tondi et al., 2006a, b; Fossen et al., 2007; Tondi, 2007; Rath et al., 2011; Rustichelli et al., 2012). Pore collapse, in fact, is an essential mechanism for their formation (e.g. Baud et al., 2009; Vajdova et al., 2010). In this regard, the fact that some compactive shear bands go through, and displace, other compactive shear bands (see Fig. 5d and Fig. 7a) poses an intriguing question. A possible solution is that compactive shear bands intersection likely occurs in the incipient phase of their formation (stage I in Fig. 12a), when porosity is not reduced below a certain value (i.e. 14%). Subsequently, both sets can simultaneously continue to accommodate shear and compaction by evolving into zones of compactive shear bands and, eventually, well-developed faults (stage II and III respectively, Fig. 12a). This process occurs because of the intrinsic properties of the carbonate grainstones (i.e. the high-porosity value, grain size and grain contact characteristics), which could easily accommodate volumetric (compaction and/or dilatation) strain. Indeed, an increased band thickness is observed at the intersecting zones, where some bands along one set diverge from the in-plane position and become parallel to the other set of bands (see Fig. 12b). This implies that, at some point, the shear displacement across the approaching band had reduced to zero before the sense of slip flip-flopped. The scenario proposed above for the development of conjugate sets of compactive shear bands represents an important difference between faulting of porous and compact (tight) rocks. In the last type of rocks, in fact, two conjugate faults cannot accommodate shear simultaneously after the initial intersection. In this regard, interested readers may compare the conceptual diagram here with those proposed by Flodin and Aydin, (2004 and Figure 14 therein) and Davatzes and Aydin (2003 and Figure 15 therein) for dilatant, pseudo-conjugate faults formed by shearing of pre-existing joints, splaying, and sequential shearing of the splays.

The evolving growth process of compactive shear bands in the porous carbonate grainstones of Cala San Nicola at Favignana is marked by distinctive values of their dimensional parameters (Fig. 12a). Single bands are typically 30–100 cm long, 4–6 mm thick and accommodate 2–4 mm of displacement. Since all data were gathered from tectonic structures crosscutting the same lithofacies (III of Fig. 2), the observed deviations can also be due to the effect of other factors such as cementation and pressure solution (Tondi, 2007), which occurred during pore collapse through grain sliding and rotation.

The zones of bands show large variations in their dimensions, and accommodate an amount of displacement proportional to the number of individual bands they include (Fig. 9). As displacement accumulated in the range of 20–30 cm, shear band development gave way to spatial localization and the formation of faults with discrete slip surfaces. These two populations of structures differ in dimensional parameters because they show breaks at about 10 cm for both thickness and displacement and at a value of about 8 m for length (Fig. 10). That data do not exactly fit the power-laws (R^2 comprised between 0.3 and 0.8) could be explained by the fact that some measurements refer to jog zones and linked faults. In fact, jogs are generally characterized by greater values of thickness for given lengths and amounts of displacement, whereas linked faults show greater length-displacement ratio similar to that reported by Cartwright et al. (1995).

The displacement-distance graphs of Fig. 8 are qualitatively similar to those of faults in compact (tight) rocks, because they both develop along-strike displacement profiles with a central maximum (e.g. Cowie and Scholz, 1992; Fossen et al., 2007). However, some differences between zones of bands and faults are evident. For example, the displacement varies along the zones of bands in relation to the number of single bands locally present. In contrast, the number of bands around faults does not increase proportionally with the displacement. Moreover, in Fig. 10a and b, the lower values of the D exponent for the faults suggest that these structures, because of the discrete slip surfaces they contain, are

Table 1
Measurements concerning maximum displacement, thickness and length of single bands, zones of bands and faults cropping out in Cala San Nicola, Favignana Island (NW Sicily, Italy).

#	Structure type	Maximum displacement (cm)	Maximum thickness (cm)	Length (cm)	Kinematic	Note
1	Single band	0.3	0.8	165	Left lateral	
2	Single band	0.2	0.4	110	Left lateral	
3	Single band	0.2	0.4	40	Left lateral	
4	Single band	0.1	0.3	43	Left lateral	
5	Single band	0.2	0.4	83	Left lateral	
6	Single band	0.2	0.4	69	Right lateral	
7	Single band	0.3	0.7	88	Right lateral	
8	Single band		0.3	35	Left lateral	
9	Single band		0.3	20	Left lateral	
10	Single band		0.8	101	Left lateral	
11	Single band		0.4	13	Left lateral	
12	Single band		0.3	35	Left lateral	
13	Single band		0.3	21	Left lateral	
14	Single band		0.5	24	Left lateral	
15	Single band		0.2	40	Left lateral	
16	Single band		0.4	19	Left lateral	
17	Single band		0.3	45	Left lateral	
18	Single band		0.6	90	Left lateral	
19	Single band		0.3	52	Left lateral	
20	Single band		0.2	21	Left lateral	
21	Single band		0.3	38	Left lateral	
22	Single band		0.5	37	Left lateral	
23	Single band		0.2	14	Left lateral	
24	Single band		0.2	21	Left lateral	
25	Single band		0.5	195	Left lateral	
26	Single band		0.4	138	Left lateral	
27	Single band		0.3	33	Left lateral	
28	Single band		0.7	130	Left lateral	
29	Single band		0.3	77	Left lateral	
30	Single band		0.6	25	Left lateral	
31	Single band		0.3	43	Left lateral	
32	Single band		0.2	55	Left lateral	
33	Single band		0.7	63	Left lateral	
34	Single band		0.5	60	Left lateral	
35	Single band		0.6	88	Left lateral	
36	Single band		0.4	38	Right lateral	
37	Single band		0.5	32	Right lateral	
38	Single band		0.2	6	Right lateral	
39	Single band		0.4	63	Right lateral	
40	Single band		0.2	68	Right lateral	
41	Single band		0.4	25	Right lateral	
42	Single band		0.2	23	Right lateral	
43	Single band		0.5	138	Right lateral	
44	Single band		0.6	146	Right lateral	
45	Single band		0.5	152	Right lateral	
46	Single band		0.6	106	Right lateral	
47	Single band		0.2	74	Right lateral	
48	Single band		0.4	63	Right lateral	
49	Zone of bands	2.2	1.1	175	Left-lateral	
50	Zone of bands	2.5	0.7	135	Left-lateral	
51	Zone of bands	3.8	1.2	160	Left-lateral	Linked
52	Zone of bands	4	2.5	200	Left-lateral	
53	Zone of bands	5.5	3.5	294	Left-lateral	
59	Zone of bands	4	5	285	Right lateral	Linked
60	Zone of bands	4	4	420	Left lateral	Linked
61	Zone of bands	3	7.5	317	Left lateral	
63	Zone of bands	6.5	15	385	Right lateral	Linked
64	Zone of bands	4	3.5		Right lateral	
65	Zone of bands	5	2.5		Right lateral	
66	Zone of bands	5.5	25		Right lateral	Linked
67	Zone of bands	4	5		Left lateral	
68	Zone of bands	10	7		Right lateral	
69	Zone of bands	13	9		Left lateral	
70	Zone of bands	9	8.5		Left lateral	
71	Zone of bands	10	9		Left lateral	
72	Zone of bands	3	2		Left lateral	
73	Zone of bands	7	21		Right lateral	
74	Zone of bands	4	4		Right lateral	
75	Zone of bands	7	6		Right lateral	
76	Zone of bands	9	7		Right lateral	
77	Zone of bands	6	4		Right lateral	
78	Zone of bands	5	9		Left lateral	

(*continued on next page*)

Table 1 (*continued*)

#	Structure type	Maximum displacement (cm)	Maximum thickness (cm)	Length (cm)	Kinematic	Note
79	Zone of bands	9	12		Left lateral	
80	Zone of bands	6	8		Left lateral	
81	Zone of bands	7	6		Right lateral	
82	Zone of bands	4	5		Right lateral	
83	Zone of bands	3	2		Left lateral	
84	Zone of bands	4	7		Left lateral	
85	Zone of bands	3.8	5		Right lateral	
86	Zone of bands	5.2	3.5		Right lateral	
87	Zone of bands	8.5	5.5		Right lateral	
88	Zone of bands	3	8		Left lateral	
89	Fault	17	7	1900	Left-lateral	Linked
90	Fault	31	12.8	1000	Right-lateral	
91	Fault	32	8	2880	Right-lateral	Linked
92	Fault	40	14	1450	Left-lateral	
93	Fault	54.5	100	9200	Left-lateral	Linked_jog zone
94	Fault	68	21	5193	Right-lateral	Linked
95	Fault	76	26	6090	Left-lateral	Linked
96	Fault	97	49	5193	Right-lateral	Linked_jog zone
54	Fault	10	11	790	Right-lateral	
55	Fault	17	7	900	Left-lateral	
56	Fault	19	11	1030	Right-lateral	
57	Fault	20	4	930	Right-lateral	
58	Fault	32	5	1480	Right-lateral	
97	Fault	140	30		Left lateral	
98	Fault	34	11		Right lateral	
99	Fault	15	7		Right lateral	
100	Fault	21	20		Right lateral	
101	Fault	30	18		Right lateral	
102	Fault	170	59		Right lateral	
103	Fault	24	21		Left lateral	
104	Fault	18	26		right lateral	
105	Fault	4.5	19		Right lateral	
106	Fault	14	10		Left lateral	
107	Fault	38	16		Left lateral	
108	Fault	16	16		Left lateral	
109	Fault	23	12		Right lateral	
110	Fault	47	40		Right lateral	
111	Fault	21	22		Right lateral	
112	Fault	50	26		Left lateral	
113	Fault	40	22		Left lateral	
114	Fault	45	40		Right lateral	
115	Fault	34	23		Right lateral	
116	Fault	20	12		Right lateral	
117	Fault	20	6		Right lateral	
118	Fault	16	14		Right lateral	
119	Fault	31	22		Left lateral	
120	Fault	24	20		Left lateral	
121	Fault	22	17		Left lateral	
122	Fault	22	12		Left lateral	
123	fault	30	26		Right lateral	
124	Fault	14	16		Right lateral	
125	Fault	24	23		Right lateral	
126	Fault	60	27		Right lateral	
127	Fault	25	16		Right lateral	
128	Fault	24	18		Right lateral	
129	Fault	15	10		Right lateral	
130	Fault	29	31		Right lateral	
131	Fault	14	10		Right lateral	
132	Fault	13	15		Left lateral	
133	Fault	13	22		Left lateral	

prone to involve larger displacements for a given thickness than the zones of bands.

Displacement-length data define two distinct groups (see Fig. 10c). The first one, which consists of single bands and zones of bands, shows a power-law scaling relation with a slope of $D = 0.5$ and, hence, a dependence of maximum displacement on the square root of discontinuity length ($D_{max} = aL^{0.5}$), similar to that documented by Fossen and Hesthammer (1997). Whereas, the second group, consisting of well-developed faults, shows a power-law scaling relation with an exponent $D = 0.7$ smaller than the expected value of $D = 1$ (Fossen et al., 2007; Schultz et al., 2008). The smaller D values for the faults D/L distribution is interpreted to result from the presence of linked faults in the fault population (see Fig. 8), which are characterized by a greater length-displacement ratio in agreement with Cartwright et al. (1995) and Nicol et al. (2010). Moreover, we believe that both single compactive shear bands and zones of compactive shear bands are characterized by a significant component of initial compaction, which sharply decreases when the threshold values for transition from shear banding to cataclastic faulting is reached (Tondi et al., 2006a, Tondi, 2007).

As far as the size-frequency datasets of Fig. 11 are concerned, several sampling biases were taken into account while interpreting

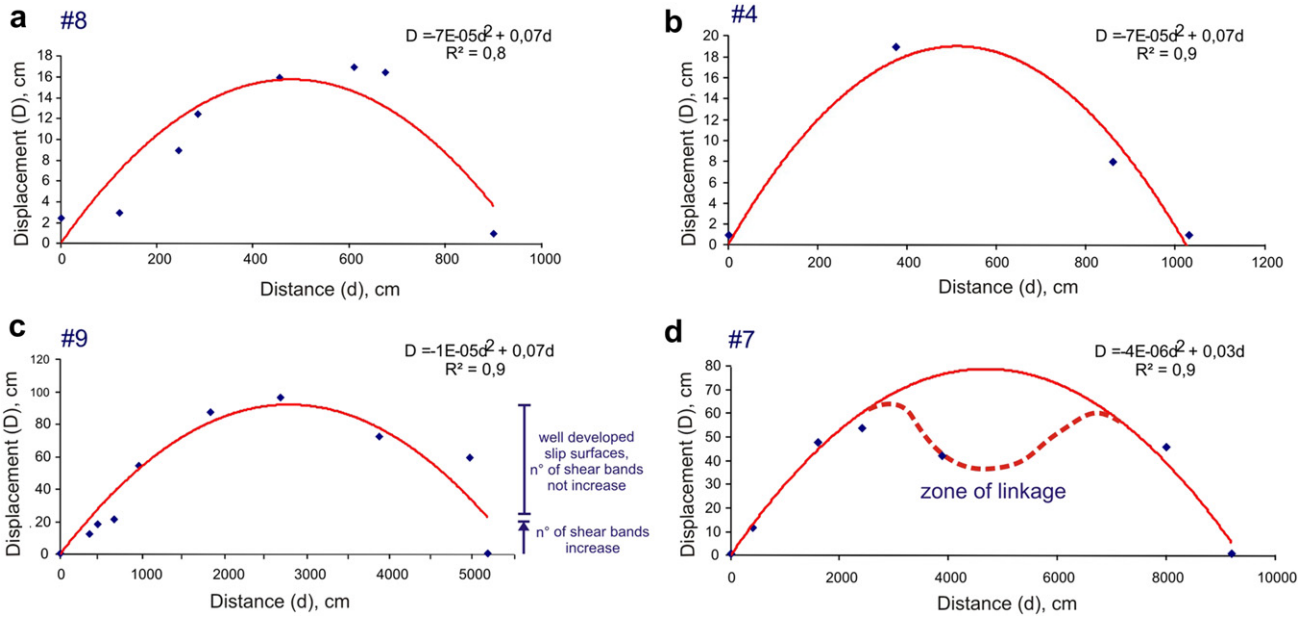

Fig. 8. Displacement-distance plots for zones of compactive shear bands with overprinted discontinuous (a, b) and continuous slip surfaces and cataclasis (c, d).

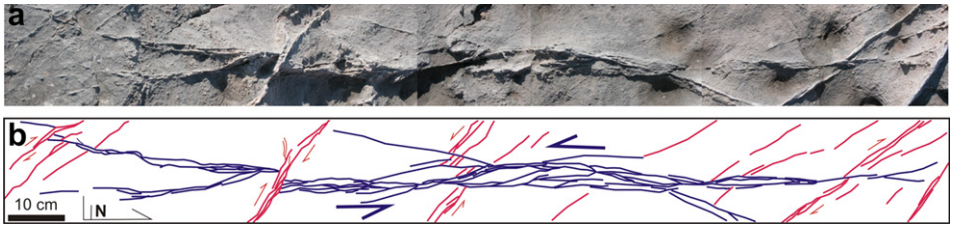

Fig. 9. N-S and NW-striking compactive shear bands; (a) photograph and (b) structural map. The greatest displacement occurs in the middle portion of the N-S striking, left-lateral zone of bands, which has a greater number of single bands relative to the tip zones.

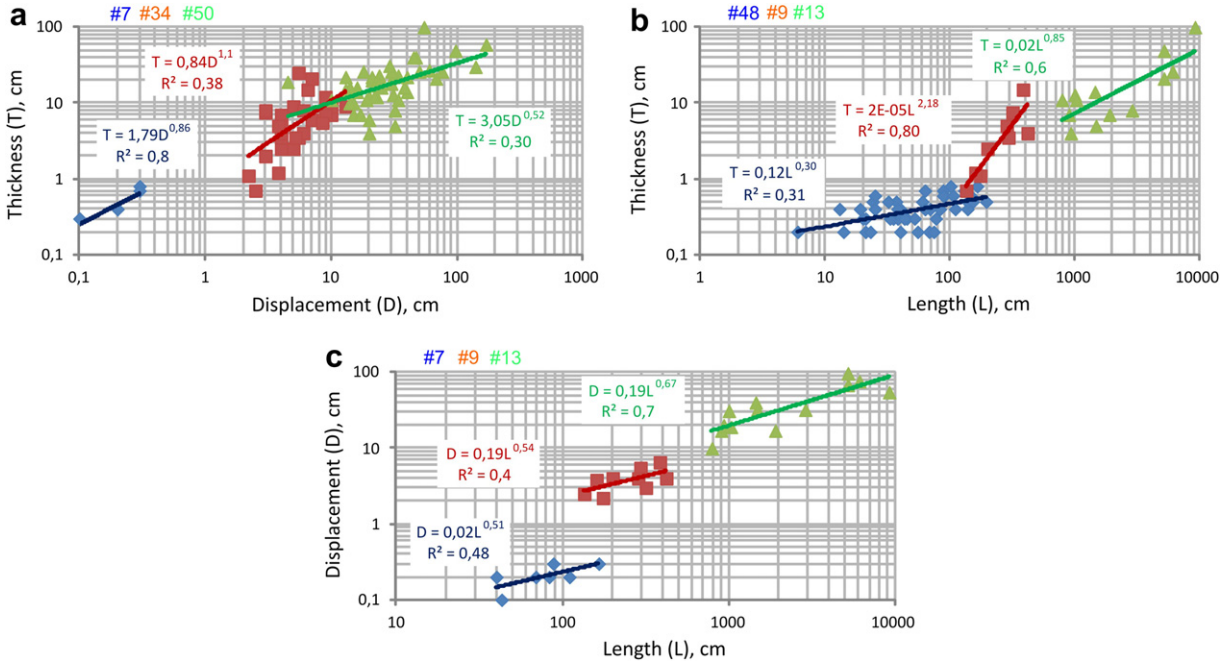

Fig. 10. Log–Log plots of (a) thickness vs. displacement, (b) thickness vs. length and (c) displacement vs. length for single bands (in blue), zones of bands (in red) and faults (in green). Best power-law fits for each structure type are also shown.

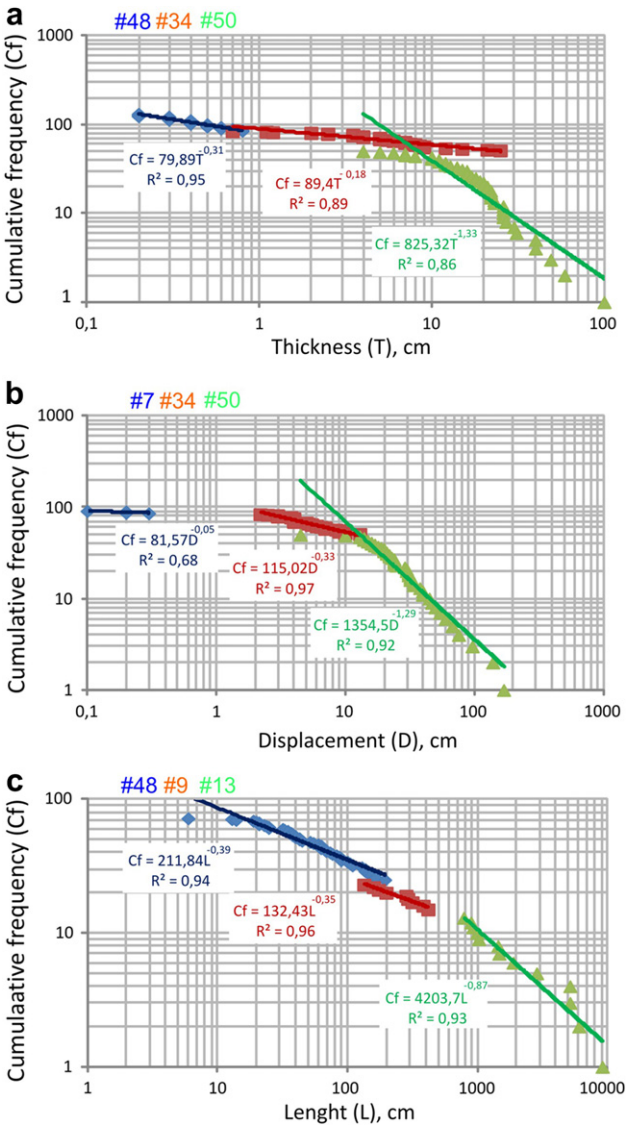

Fig. 11. Cumulative frequency distributions of thickness (a), displacement (b), and length (c) computed for single bands (in blue), zones of bands (in red) and faults (in green). The resolution limits are 0.5 mm for both thickness and displacement and 1 mm for the length.

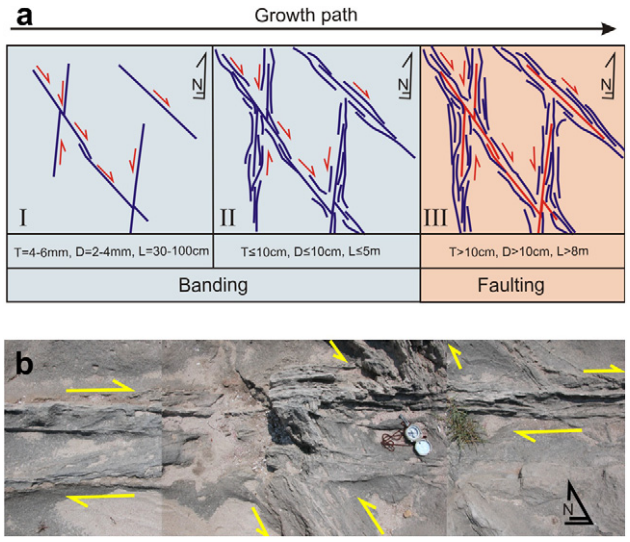

Fig. 12. (a) Conceptual model for conjugate strike-slip compactive shear bands developed in the Lower Pleistocene porous carbonate grainstones of Favignana Island (NW Sicily). In the Stage III, slip surfaces are marked in red. The transition from one deformation mechanism to another (i.e. banding vs. faulting) is recorded by the changes in maximum thickness (T), displacement (D) and length (L) of the different structure types. (b) Example of an intersecting zone between the conjugate sets of compactive shear bands. Please note the increased thickness of the band zones at this location. The compass is 20 cm long.

the statistical distributions. First, small-scale data are usually underestimated due to the limits of resolution of the methods used for the data acquisitions. This effect is called truncation (Einstein and Baecher, 1983; Barton and Zoback, 1992; Pickering et al., 1995). Second, the abundance of large-scale data can be significantly underestimated. This effect is called censoring (Einstein and Baecher, 1983; Yielding et al., 1992) and may have several causes. Of particular concern, censoring is related to the size of the survey. For example, fault lengths larger than this particular size are not sampled and can be underestimated.

In the case of measurements in the present study, the observable censoring of the data for faults, which is particularly evident as regards the lengths, is due to the size of the outcrop. In fact, this occurs because our sample site of a small promontory located along the coastal line has many of the largest faults with one of the two tips located offshore. Moreover, data truncation is particularly evident on the displacement and thickness distributions of faults and on the lengths of single bands, and can be related to the range of values for which measurements are achieved. In fact, if values are close to the switching values between one data sets to another (i.e. zones of bands and faults), data belonging to one single data set can be underestimated. This is evident in Fig. 11a and b, where around values of 10 cm of both thickness and displacement, the distributions got zones of bands and faults overlap. Moreover, the calculated power law relationships cover less than one order of magnitude of the size range (Fig. 11). Still this approach of defining several power law segments over short ranges to fit complex statistical distributions is not uncommon in the literature (Berkowitz and Hadad, 1997; Wojtal, 1996; Fossen and Rørnes, 1996).

Even allowing for the aforementioned limitations in the statistical analysis, we believe that the results highlight the transition from one deformation behavior to another (i.e. banding vs. faulting). In fact, clear breaks are visible in Fig. 11a and b between the two populations of structures comprising: (i) single bands and zones of bands, and (ii) faults. These variations, moreover, are similar to those showing evolution of the distribution of dimensional parameters of joint systems as a function of their progressive development (Rives et al., 1992; Wu and Pollard, 1995). Finally, the cumulative distributions computed for the faults are quite similar to the data previously published in the literature (Marrett and Allmendinger, 1992; Walsh and Watterson, 1992; Villemin et al., 1995; Tondi and Cello, 2003).

5. Conclusions

In this paper we investigated the growth modes, dimensional properties and scaling relationships of one pair of high-angle to bedding conjugate sets of compactive shear bands, characterized by strike-slip kinematics, crosscutting Lower Pleistocene carbonate grainstones of Favignana Island, NW Sicily. Similar to the results from previous studies, we found that the compactive shear bands nucleate as single bands, may evolve into zones of compactive shear bands, and, eventually, into faults with discrete slip surfaces and cataclastic fault rocks. We documented that the transition from one deformation behavior to another (i.e. banding vs. faulting) is recorded by different values of the dimensional parameters (i.e.

length, thickness, displacement) that characterize the individual tectonic structures (single bands, zones of bands, faults), as well as their ratios and distributions. In particular: (i) single bands are generally 30–100 cm long, 4–6 mm thick and resolve 2–4 mm of displacement. Thickness vs. displacement and displacement vs. length relations are nicely expressed by power-law best fits in log–log diagrams, whereas thickness vs. length does not appear to have a well defined relationship; (ii) zones of bands are maximum 5 m long, 10 cm thick and have up to 10 cm of displacement. The two last parameters are related to the number of bands comprised within the zones; (iii) displacement and thickness are maximum at approximately midpoint or in the central part of both zones of bands and faults; (iv) displacement vs. length data define two distinct trends for each group of structure. The first group, consisting of single bands and zones of bands, shows a power-law scaling relation with a slope of $D = 0.5$ in a log–log diagram, and hence a dependence of maximum displacement on the square root of length. The second group, represented by faults, shows a power-law scaling relation with a slope of $D = 0.7$. These two groups of structures, moreover, display clear breaks in the cumulative frequency distributions of their dimensional parameters.

Aside from the scientific implications of our results, they may also be helpful in applications such as geofluids management for improving the forecasting of carbonate reservoir quality by mapping/simulating/assessing shear bands dimension and distribution and understanding the extent of reservoir compartmentalization. Indeed, the preliminary permeability measurement conducted on samples collected from our faults show values of the order of 10^{-19} m^2 for cross-fault flow and 10^{-17} m^2 for along fault flow (Faulkner's personal communication). These values, whose meaning and detailed characterization will be investigated in the future) are few order of magnitude less than the host rock permeability values ($>10^{-15}$). A clear dependence of the fluid flow paths through porous carbonate reservoirs on the orientation, density and connectivity of shear band faults is therefore suggested by the aforementioned permeability data.

Acknowledgments

This work has been supported by the Reservoir Characterization Project (www.rechproject.com), the MIUR-PRIN 2009, and the Rock Fracture Project at Stanford University. We are grateful to D. Faulkner from the Rock Deformation Laboratory of Liverpool for the permeability measurements. We acknowledge the comments and suggestions provided by the editor W.M. Dunne and by the two reviewers, N. Dawers and H. Fossen, whose comments improved both quality and legibility of this paper.

Appendix. Supplementary material

Supplementary data related to this article can be found online at doi:10.1016/j.jsg.2012.02.003.

References

Abate, B., Ferruzza, G., Incandela, A., Renda, P., 1995. Tettonica trascorrente nelle isole Egadi (Sicilia Occidentale). Studi Geologici Camerti, 9–14.
Abate, B., Incandela, A., Renda, P., 1997. Carta Geologica delle Isole di Favignana e Levanzo. Dipartimento di Geologia, University of Palermo.
Agosta, F., Alessandroni, M., Antonellini, M., Tondi, E., Giorgioni, M., 2010. From fractures to flow: a field-based quantitative analysis of an outcropping carbonate reservoir. Tectonophysics 490, 197–213.
Agosta, F., Alessandroni, M., Tondi, E., Aydin, A., 2009. Oblique-slip normal faulting along the northern edge of the Majella anticline: inferences on hydrocarbon migration and accumulation. Journal of Structural Geology 31, 690–774.
Ahlgren, S.G., 2001. The nucleation and evolution of Riedel shear-zones as deformation bands in porous sandstone. Journal of Structural Geology 23, 1203–1214.
Antonellini, A., Tondi, E., Ago sta, F., Aydin, A., Cello, G., 2008. Failure modes in basin carbonates and their impact on fault development, Majella Mountain, central Italy. Marine and Petroleum Geology 25, 1074–1096.
Antonellini, M.A., Aydin, A., 1994. Effect of faulting on fluid flow in porous sandstones: petrophysical properties. American Association of Petroleum Geologists Bulletin 78, 355–377.
Antonellini, M.A., Aydin, A., 1995. Effect of faulting on fluid flow in porous sandstones: geometry and spatial distribution. American Association of Petroleum Geologists Bulletin 79, 642–671.
Aydin, A., 1978. Small faults formed as deformation bands in sandstone. Pure and Applied Geophysics 116, 913–930.
Aydin, A., Johnson, A.M., 1978. Development of faults as zones of deformation bands and as slip surfaces in sandstone. Pure and Applied Geophysics 116, 931–942.
Aydin, A., Johnson, A.M., 1983. Analysis of faulting of porous sandstone. Journal of Structural Geology 5 (1), 1931. http://dx.doi.org/10.1016/0191-8141(83)90004-4.
Aydin, A., Borja, R.I., Eichhubl, P., 2006. Geological and mathematical framework for failure modes in granular rock. Journal of Structural Geology 28, 83–98.
Baud, P., Klein, E., Wong, T.F., 2004. Compaction localization in porous sandstones: spatial evolution of damage and acoustic emission activity. Journal of Structural Geology 26, 603–624.
Baud, P., Vinciguerra, S., David, C., Cavallo, A., Walker, E., Reuschlé, T., 2009. Compaction and failure in high porosity carbonates: mechanical data and microstructural microstructural observations. Pure and Applied Geophysics 166, 869–898.
Barton, C.A., Zoback, M.D., 1992. Self-Similar Distribution and Properties of Macroscopic Fractures at Depth in Crystalline Rock in the Cajon Pass Scientific Drill Hole. J. Geophys. Res 97 (B4), 5181–5200. doi:10.1029/91JB01674.
Baxevanis, T., Papamichos, E., Flornes, O., Larsen, I., 2006. Compaction bands and induced permeability reduction in Tuffeau de Maastricht calcarenite. Acta Geotechnica 1, 123–135.
Berkowitz, B., Hadad, A., 1997. Fractal and multifractal measures of natural and synthetic fracture networks. Journal of Geophysical Research 102, 12205–12218.
Cartwright, J.A., Trudgill, B.D., Mansfeld, C.S., 1995. Fault growth by segment linkage: an explanation for scatter in maximum displacement and trace length data from the Canyonlands Grabens of SE Utah. Journal of Structural Geology 17, 1319–1326.
Childs, C., Walsh, J.J., Watterson, J., 1990. A method for estimation of the density of fault displacements below the limits of seismic resolution in reservoir formations. In: Buller, A.T., Berg, E., Hjelmeland, O., Kleppe, J., Torsaeter, O., Aasen, J.O. (Eds.), North Sea Oil and Gas Reservoirs: II. Proceedings of the North Sea Oil and Gas Reservoirs Conference, pp. 309–318.
Cilona, A., Baud, P., Tondi, E., Agosta, F., Vinciguerra, S., Rustichelli, A., Spiers, C.J., 2011. Deformation bands in porous carbonate grainstones: field and laboratory observations. Journal of Structural Geology. Submitted for publication.
Cowie, P.A., Scholz, C.H., 1992. Displacement-length scaling relationship for faults: data synthesis and discussion. Journal of Structural Geology 14, 1149–1156.
Davatzes, N.C., Aydin, A., 2003. The formation of conjugate normal fault systems in folded sandstone by sequential jointing and shearing, Waterpocket Monocline, Utah. Journal of Geophysical Research 108 (B10), 2478.
Dawers, N.H., Anders, M.H., Scholz, C.H., 1993. Growth of normal faults: displacement-length scaling. Geology 21, 1107–1110.
de Joussineau, G., Aydin, A., 2007. The evolution of the damage zone with fault growth in sandstone and its multiscale characteristics. Journal of Geophysical Research 112 (B12401), 19. doi:10.1029/2006JB004711.
Eichhubl, P., Hooker, J.N., Laubach, S.E., 2010. Pure and shear-enhanced compaction bands in Aztec sandstone. Journal of Structural Geology 32, 1873–1886.
Einstein, H.H., Baecher, G.B., 1983. Probabilistic and statistical methods in engineering geology, specific methods and examples Part I: exploration. Rock Mechanics and Rock Engineering 16, 39–72.
Engelder, T., 1974. Cataclasis and the generation of fault gouge. Geological Society of America Bulletin 85, 1515–1522.
Ferrill, D.A., Groshong Jr., R.H., 1993. Deformation conditions in the northern Subalpine Chain, France, estimated from deformation modes in coarse-grained limestone. Journal of Structural Geology 15, 995–1006.
Flodin, E.A., Aydin, A., 2004. Evolution of a strike-slip fault network, Valley of Fire, southern Nevada. Geological Society of America Bulletin 116 (1/2), 42–59.
Fossen, H., Hesthammer, J., 1997. Geometric analysis and scaling relations of deformation bands in porous sandstone. Journal of Structural Geology 19, 1479–1493.
Fossen, H., Schultz, R.A., Anita, T., 2011. Conditions and implications for compaction band formation in the Navajo Sandstone, Utah. Journal of Structural Geology 33, 1477–1490.
Fossen, H., Schultz, R.A., Shipton, Z.K., Mair, K., 2007. Deformation bands in sandstone: a review. Journal of the Geological Society 164, 755–769.
Fossen, H., Rørnes, A., 1996. Properties of fault populations in the Gullfaks Field, northern North Sea. Journal of Structural Geology 18. 2–3, 179–190.
Giunta, G., Luzio, D., Tondi, E., De Luca, L., Giorgianni, A., D'Anna, G., Renda, P., Cello, G., Nigro, F., Vitale, M., 2004. The Palermo (Sicily) seismic cluster of September 2002, in the seismotectonic framework of the Tyrrhenian Sea–Sicily border area. Annals of Geophysics 47 (6), 1755–1770.
Giunta, G., Nigro, F., Renda, P., Giorgianni, A., 2000. The Sicilian–Maghrebides Tyrrhenian margin: a neotectonic evolutionary model. Bollettino della Società Geologica Italiana 119, 553–565.

Giunta, G., Luzio, D., Agosta, F., Calò, M., Di Trapani, F., Giorgianni, A., Oliveri, E., Orioli, S., Perniciaro, M., Vitale, M., Chiodi, M., Adelfio, Giada, 2009. An integrated approach to investigate the seismotectonics of northern Sicily and southern Tyrrhenian. Tecto 476, 13–21. doi:10.1016/j.tecto.2008.09.03.

Gueguen, E., Tavarnelli, E., Renda, P., Tramutoli, M., 2002. The geodynamics of the southern Tyrrhenian Sea margin as revealed by integrated geological, geophysical and geodetic data. Bollettino della Società Geologica Italiana 1, 77–85.

Incandela, A., 1995. Deformazioni neogeniche nelle isole di Favignana e Levanzo. Memorie della Società Geologica Italiana 51 (6), 129–135.

Katz, Y., Weinberger, R., Aydin, A., 2004. Geometry and kinematic evolution of Riedel shear structures, Capitol Reef National Park, Utah. Journal of Structural Geology 26 (3), 491–501.

Mandelbrot, B.B., 1983. The Fractal Geometry of Nature. W. H. Freeman, San Francisco.

Marrett, R., Allmendinger, R.W., 1992. Amount of extension on "small" faults: an example from the Viking Graben. Geology 20, 47–50.

Micarelli, L., Benedicto, A., Wibberley, C.A.J., 2006. Structural evolution and permeability of normal fault zones in highly porous carbonate rocks. Journal of Structural Geology 28, 1214–1227.

Nicol, A., Walsh, J.J., Villamor, P., Seebeck, H., Berryman, K.R., 2010. Normal fault interactions, paleoearthquakes and growth in an active rift. Journal of Structural Geology 32, 1101–1113.

Nigro, F., Renda, P., Arisco, G., 2000. Tettonica recente nella Sicilia nord-occidentale e nelle Isole Egadi. Bollettino della Società Geologica Italiana 119, 307–319.

Pickering, G., Bull, J.M., Sanderson, D.J., 1995. Sampling power-law distributions. Tectonophysics 248, 1–20.

Pittman, E.D., 1981. Effect of fault-related granulation on porosity and permeability of quartz sandstones, Simpson Group (Ordovician), Oklahoma. American Association of Petroleum Geologists Bulletin 65, 2381–2387.

Rath, A., Exner, U., Tschegg, C., Grasemann, B., Laner, R., Draganits, E., 2011. Diagenetic control of deformation mechanisms in deformation bands in a carbonate grainstone. AAPG Bulletin 95 (8), 1369–1381.

Renda, P., Tavarnelli, E., Tramutoli, M., Gueguen, E., 2000. Neogene deformations of Northern Sicily, and their implications for the geodynamics of the Southern Tyrrhenian Sea margin. Memorie della Società Geologica Italiana 55, 53–59.

Rives, T., Razack, M., Petit, J.P., Rawnsley, K.D., 1992. Joint spacing - analog and numerical simulations. Journal of Structural Geology 14 (8–9), 925–937.

Rustichelli, A., Tondi, E., Agosta, F., Cilona, A., and Giorgioni, M., 2012. Development and distribution of bed-parallel compaction bands and pressure solution seams in the Bolognano Formation carbonates (Majella Mountain, Italy). Journal of Structural Geology, in press doi:10.1016/j.jsg.2012.01.007.

Scandone, P., Giunta, G., Liguori, V., 1974. The connection between Apulia and Sahara continental margins in the Southern Apennines and in Sicily. Memorie della Società Geologica Italiana 13, 317–323.

Scholz, C.H., 2002. The Mechanics of Earthquakes and Faulting, second ed. Cambridge University Press, Cambridge.

Scholz, C.H., Cowie, P.A., 1990. Determination of total strain from faulting using slip measurements. Nature 346, 837–839.

Schultz, R.A., Soliva, R., Fossen, H., Okubo, C.H., Reeves, D.M., 2008. Dependence of displacement–length scaling relations for fractures and deformation bands on the volumetric changes across them. Journal of Structural Geology 30, 1405–1411.

Shipton, Z.K., Evans, J.P., Thompson, L.B., 2005. The geometry and thickness of deformation-band fault core and its influence on sealing characteristics of deformation-band fault zones. In: Sorkhabi, R., Tsuji, Y. (Eds.), Faults, Fluid Flow, and Petroleum Traps, vol. 85. AAPG Memoir, pp. 181–195.

Shipton, Z.K., Cowie, P.A., 2001. Analysis of three-dimensional damage zone development over m to km scale range in the high-porosity Navajo sandstone, Utah. Journal of Structural Geology 23, 1825–1844.

Shipton, Z.K., Cowie, P.A., 2003. A conceptual model for the origin of fault damage zone structures in high-porosity sandstone. Journal of Structural Geology 25, 333–344. http://dx.doi.org/10.1016/S0191-8141(02)00037-8.

Tavarnelli, E., Renda, P., Pasqui, V., Tramutoli, M., 2003. Composite structures resulting from negative inversion: an example from the Isle of Favignana (Egadi Islands). Bollettino Della Societa Geologica Italiana 122 (7), 319–325.

Tondi, E., Zampieri, D., Giunta, G., Renda, P., Unti, M., Giorgianni, A., Cello, G., 2006b. Active faults and inferred seismic sources in the San Vito lo Capo peninsula, north-western Sicily, Italy. In: Geological Society, London, Special Publications, vol. 262, pp. 365–377.

Tondi, E., 2007. Nucleation, development and petrophysical properties of faults in carbonate grainstones: evidence from the San Vito Lo Capo peninsula (Sicily, Italy). Journal of Structural Geology 29, 614–628.

Tondi, E., Antonellini, M., Aydin, A., Marchegiani, L., Cello, G., 2006a. The role of deformation bands and pressure solution seams in fault development in carbonate grainstones of the Majella Mountain, Italy. Journal of Structural Geology 28, 376–391.

Tondi, E., Cello, G., 2003. Spatiotemporal evolution of the central Apennines fault system (Italy). Journal of Geodynamics 36, 113–128.

Vajdova, V., Baud, P., Wong, T.-F., 2004. Compaction, dilatancy, and failure in porous carbonate rocks. Journal of Geophysical Research 109, B05204.1–B05204.16.

Vajdova, V., Baud, P., Wu, L., Wong T.-F. Micromechanics of inelastic compaction in two allochemical limestones. Journal of Structural Geology, 33, Submitted for publication.

Vajdova, V., Zhu, W., Chen, T.-M.N., Wong, T.-f., 2010. Micromechanics of brittle faulting and 997 cataclastic flow in Tavel limestone. Journal of Structural Geology 32, 1158–1169.

Villemin, T., Angelier, J., Sunwoo, C., 1995. Fractal distribution of fault length and displacements: implications of brittle deformation evaluation: the Lorraine coal basin. In: Barton, C.C., La Pointe, P.R. (Eds.), Fractals in the Earth Sciences. Plenum Press, New York, pp. 205–226.

Walsh, J.J., Watterson, J., 1992. Populations of faults and fault displacements and their effects on estimates of fault-related regional extension. Journal of Structural Geology 14, 701–712.

Wibberley, C.A.J., Petit, J.-P., Rives, T., 2000. Mechanics of cataclastic 'deformation band' faulting in high-porosity sandstone, Provence. Comptes Rendus de l'Academie des Sciences, Serie IIA 331, 419–425.

Willemse, E.J.M., Pollard, D.D., Aydin, A., 1996. Three-dimensional analyses of slip distributions on normal fault arrays with consequences for fault scaling. Journal of Structural Geology 18 (2/3), 295–909.

Wojtal, S.F., 1996. Changes in fault displacement populations correlated to linkage between faults. Journal of Structural Geology 18. 2–3, 265–279.

Wu, H., Pollard, D.D., 1995. An experimental study of the relationship between joint spacing and layer thickness. Journal of Structural Geology 17 (6), 887–905.

Yielding, G., Walsh, J.J., Watterson, J., 1992. The prediction of small-scale faulting in reservoirs. First Break 10, 449–460.

Zhu, W., Baud, P., Wong, T.-F., 2010. Micromechanics of cataclastic pore collapse in limestone. Journal of Geophysical Research 115, B04405.1–B04405.17.